

Compact in-line lensfree digital holographic microscope

Manon Rostykus, Ferréol Soulez, Michael Unser, Christophe Moser

▶ **To cite this version:**

Manon Rostykus, Ferréol Soulez, Michael Unser, Christophe Moser. Compact in-line lensfree digital holographic microscope. Methods, 2018, 136, pp.17-23. 10.1016/j.ymeth.2017.11.008 . insu-01696945

HAL Id: insu-01696945
https://insu.hal.science/insu-01696945

Submitted on 30 Jan 2018

HAL is a multi-disciplinary open access archive for the deposit and dissemination of scientific research documents, whether they are published or not. The documents may come from teaching and research institutions in France or abroad, or from public or private research centers.

L'archive ouverte pluridisciplinaire **HAL**, est destinée au dépôt et à la diffusion de documents scientifiques de niveau recherche, publiés ou non, émanant des établissements d'enseignement et de recherche français ou étrangers, des laboratoires publics ou privés.

Methods xxx (2017) xxx–xxx

Contents lists available at ScienceDirect

Methods

journal homepage: www.elsevier.com/locate/ymeth

Compact in-line lensfree digital holographic microscope

Manon Rostykus [a,*], Ferréol Soulez [b,c], Michael Unser [b], Christophe Moser [a]

[a] Laboratory of Applied Photonics Devices, École Polytechnique Fédérale de Lausanne (EPFL), Lausanne, Switzerland
[b] Biomedical Imaging Group, École Polytechnique Fédérale de Lausanne (EPFL), Lausanne, Switzerland
[c] Univ Lyon, Univ Lyon1, Ens de Lyon, CNRS, Centre de Recherche Astrophysique de Lyon UMR5574, F-69230 Saint-Genis-Laval, France

ARTICLE INFO

Article history:
Received 15 September 2017
Received in revised form 13 November 2017
Accepted 16 November 2017
Available online xxxx

ABSTRACT

Phase imaging provides intensity contrast to visualize transparent samples such as found in biology without any staining. Among them, digital holographic microscopy (DHM) is a well-known quantitative phase method. Lensfree implementations of DHMs offer the added advantage to provide large field of views (several mm^2 compared to several hundred μm^2) and more compact setups that traditional DHM which have high quality microscope objectives. In this article, a lensfree DHM is presented using a side illumination technique in order to further reduce the device size. Its practical use is described and results on a transparent (phase only) sample are shown.

© 2017 Published by Elsevier Inc.

1. Introduction

Imaging transparent objects is an important challenge for biology since cells are mostly transparent to visible and infrared light. Phase imaging allows imaging such objects without any prior staining of the sample. Different modalities exist. Phase contrast microscopy [1] and differential interference contrast (DIC) microscopy are two of the most spread techniques. They are based on the conversion of the phase changes due to the sample, which cannot be seen, into intensity changes that can be observed by eye or with a visible camera. Without additional modifications, these techniques do not give quantitative information about the phase shift, i.e. the optical thickness of the cell (the product of index of refraction by the cell thickness); they only allow visualization.

Digital holographic microscopy (DHM) is based on recording a hologram of the sample. The latter is then reconstructed digitally in order to retrieve the amplitude and phase of the sample. It is a quantitative phase imaging technique, which means that transparent objects cannot only be visualized but quantitative information about the optical thickness (i.e. morphology) can be extracted with nanometer precision [2–7]. It is thus a label-free method which does not require the kind of staining used in fluorescent microscopy [8]. The DHM technique also allows for real time data recording, such as to view the damage or the repair of cells in real time during laser microsurgery [9], observe cell division [10] or changes of cellular volume to monitor apoptosis for example [4,5,11–14]. During the digital image reconstruction, the object can be retrieved at different focal planes which makes 3D tracking of particles/cells possible [2,15–19]. The observation of neuronal network activity also paves the way to functional imaging using DHM [20]. Finally biophysical parameters such as intra cellular refractive index are accessible [4,5,12,13] and dried mass concentration [21].

DHM has also been developed without any microscope objective or lenses in order to obtain a simpler setup. Those devices are made of the same three parts as a classical microscope: illumination, a sample on a slide and a detector; however the detection part only contains a camera; no optical element is situated between the sample and the camera. This makes the microscope more compact and cheaper. Such compact lensless setups can be used to monitor cellular growth directly within the incubator. Another advantage is the field of view (FOV) which is equal to the size of the camera chip (∼several mm^2). Most implementations use in-line digital holography [22–24]. The existing setups use partially coherent light (LEDs) in order to have less noisy images by limiting speckle and to be cost effective. However the compactness is impacted by the need of obtaining a certain degree of spatial coherence. Indeed, an inline setting uses a small distance between the cell plane and the camera chip (z2) and a large distance (z1) between the source and the cell plane [22]. This allows using a LED source with a pinhole of the order of 50 μm and obtaining a large FOV. The sum of the distance from pinhole to camera (z1 + z2) is the same as for typical inline holographic setup with large spatial coherence length. In the latter, the z2 is large and z1 is small. The partially coherent illumination is restricted to samples containing objects smaller or equal to the spatial coherence disk at the sample, which is typically 500–1000 times the wavelength. Since a highly coherent source is used in our implementation, we are not limited to have a small z1 (which is the case for LEDs to

* Corresponding author.
E-mail address: manon.rostykus@epfl.ch (M. Rostykus).

https://doi.org/10.1016/j.ymeth.2017.11.008
1046-2023/© 2017 Published by Elsevier Inc.

obtain a minimum spatial coherence). Hence, by placing the cell plane close the camera plane (small z2), the fringe magnification is close to 1 and the FOV is the illuminated area (chip). Effectively, the coherent point source is collimated by the analog hologram which creates a secondary illumination making the distance z1 and z2 small. Inline holography requires, in most cases, more than one hologram to retrieve the quantitative phase information of the sample (in the previous described concepts for off-axis DHM, only one hologram was required). However, if a phase image is wanted, one image is sufficient (but the quantitative phase is lost).

In the present paper, we present a lensfree DHM where the novelty resides in the side illumination which reduces the height of a lensfree DHM by one order of magnitude. The compact in-line lensfree digital holographic microscope is described in Section 2. Then more practical details are given in Section 3. Results on biological cells are shown in Section 4. Section 5 contains discussion and conclusion.

2. Compact in-line digital lensfree holographic microscope description

2.1. Working principle

The proposed device is based on in-line digital holography. This technique consists in illuminating the sample with a coherent or partially coherent light, such as from a laser for example. After the sample, the light is decomposed in two parts: one disturbed part and one undisturbed part as shown in Fig. 1. The disturbed part (also known as scattered part) is the part of the light that has been scattered by the transparent sample and the undisturbed part is the part of the light that goes through without "seeing" the sample. Both parts are coherent with each other and interfere at the camera plane. This interference pattern is sampled and digitized by the chip to gives the so-called in-line hologram. The 3D information of the object is contained in this intensity image.

In order to retrieve the quantitative amplitude and phase of the sample, phase retrieval algorithms [25,26] require more than one hologram. This is due to the well-known twin-image problem. Indeed, the real, virtual and zero order images are superimposed in the spectrum, which implies that the image is disturbed by the out-of-focus twin-image [25] and the phase cannot be retrieved correctly. This twin-image problem arises from the intensity-only measurements and the subsequent loss of the phase. Fig. 2 shows a simulation of inline holography. The ground truth consists of human epithelial cells on a microscope slide have been imaged using a commercial DHM from LynceeTec. The reconstructed amplitude and phase of the cells measured with the DHM are then used to simulate inline holography. Fig. 2(a) is the original amplitude and Fig. 2(b) is the original phase. These two are combined to make a simulated hologram. Fig. 2(c) (resp. Fig. 2(d)) shows the reconstructed amplitude (resp. phase) using only backpropagation of one hologram. The twin image is clearly visible creating ringing structures around objects.

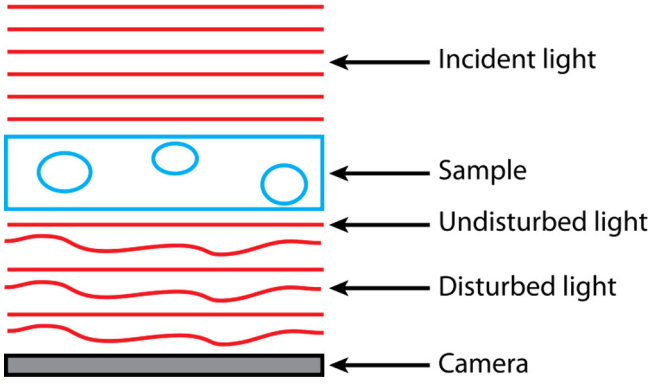


Fig. 1. Sketch of in-line digital hologram recording.

This twin-image problem is characteristic of in-line holography. One way to avoid it is to use off-axis holography has been primarily developed to avoid this problem. This technique consists in illuminating the sample with one beam that interferes coherently with a second beam that does not go through the sample and makes an angle with the first beam. The real image, virtual image and zero order are then separated in the spectrum, which allows retrieving a twin-image free image and a correct phase with simple spectrum filtering and backpropagation algorithm. Compact off-axis DHM have already been presented, either as a device to be inserted in a classical microscope [27], or as a portable device that uses a grating to redirect part of the incident light to create a reference beam with a specific angle [28–30]. This technique still limits the compactness and/or the FOV due to the necessary angle between the two beams to have interference fringes resolved by a camera with specific pixel size and the fact that the reference beam should not go through the sample part.

In inline holography, this twin image problem is solved numerically by the mean of phase retrieval algorithms. They estimate both phase and intensity from intensity only holograms using additional information. This can be prior knowledge about the sample as support constraints [31–35]. The required information can also be gathered by recording several holograms of the same sample with for instance different distances between the sample and the camera [36,37], different light source wavelengths [38], or by illuminating the sample with different illumination directions [24,39]. The last method is used in the proposed device.

2.2. Device

The proposed device is made of 3 elements: a vertical-cavity surface-emitting lasers (VCSELs) array, a prism and a camera. Fig. 3 shows a schematic of the device with all the components. The total height of the device is ~10 mm for a FOV of ~17 mm^2.

The array of sources is placed in front of the entrance surface of the prism. Each VCSEL is single-mode with a wavelength of 673 nm and a linewidth of 100 MHz (Vixar 680S). They consume low power (~1 mW) which makes them suitable for a battery operated device.

On the longest surface of the K9 prism, a photopolymer BAYFOL®HX is laminated. This material is sensitive to light: it changes its refractive index according to the amount of light it receives. Thanks to this property phase (transparent) volume hologram gratings can be recorded inside. A grating is used to redirect the light from one direction to another direction. Several gratings are recorded in the photopolymer. The sequential recording process is described in Ref. [24]. For each VCSEL corresponds one hologram grating which diffracts its light out of the prism with a specific angle. The diffracted light goes through the sample and the inline hologram is recorded by the camera. The angular scanning is performed in 2D.

The camera is a complementary metal-oxidesemiconductor (CMOS) sensor with 5.2 μm pixel size (Thorlabs DCC1545M).

3. Compact in-line DHM in practice

Image acquisition and reconstruction steps are depicted in Fig. 4.

3.1. Image acquisition

In the presented results only one VCSEL on a translation stage was used. The system can be made more practical, instead of trans-

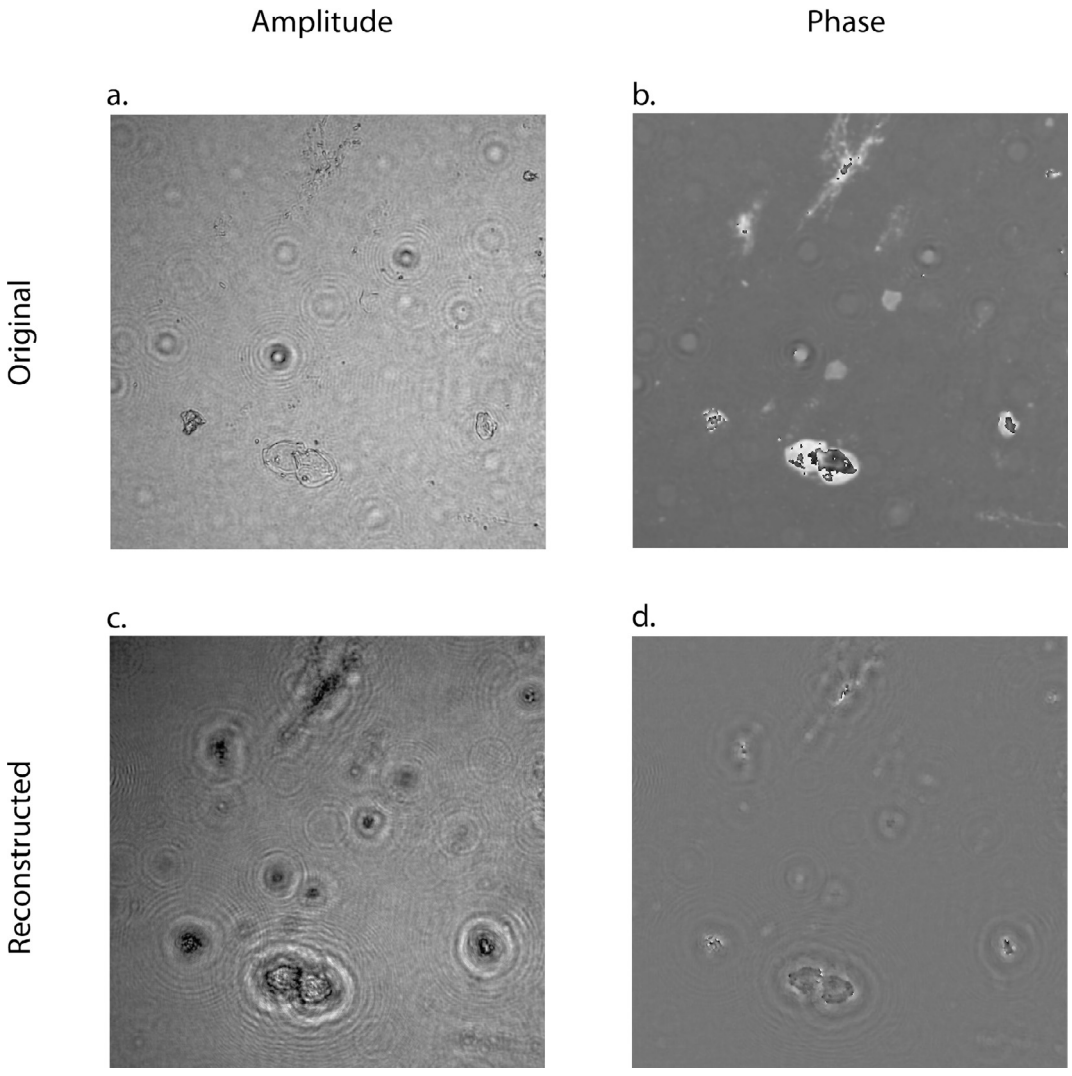


Fig. 2. Simulated backpropagation with an in-line hologram. (a) Original object amplitude. (b) Original object phase. (c) reconstructed amplitude using backpropagation algorithm with only one simulated hologram. (d) Reconstructed phase using backpropagation algorithm with only one simulated hologram.

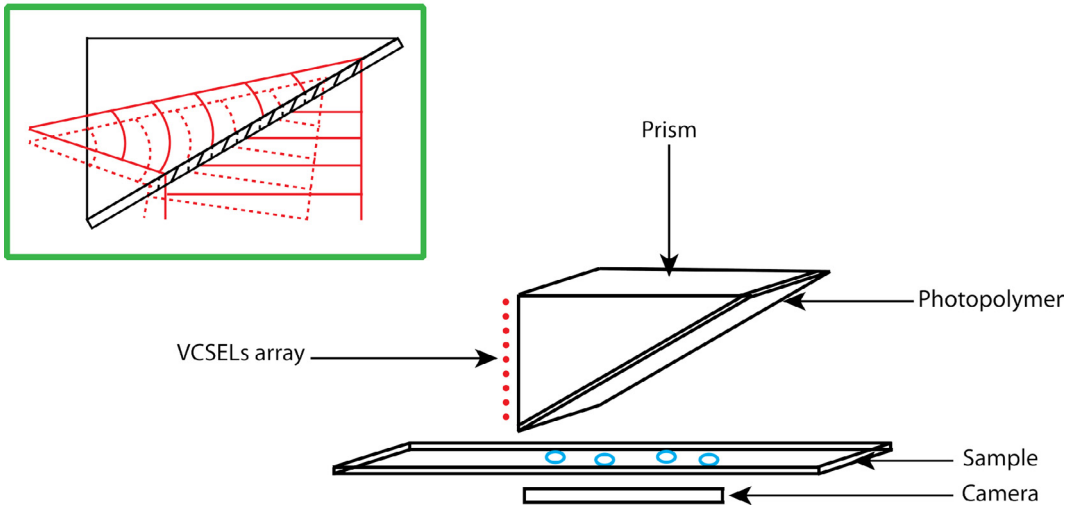


Fig. 3. Scheme of the compact in-line lensfree digital holographic microscope. The distance between the sample and the lower edge of the prism is less than 1 mm, as well as between the sample and the camera. The prism is 2 cm × 1.7 cm × 1 cm. The green inset shows the diffraction of two different illumination angles with two different gratings. The wavefront shaping is also depicted. (For interpretation of the references to colour in this figure legend, the reader is referred to the web version of this article.)

Please cite this article in press as: M. Rostykus et al., Methods (2017), https://doi.org/10.1016/j.ymeth.2017.11.008

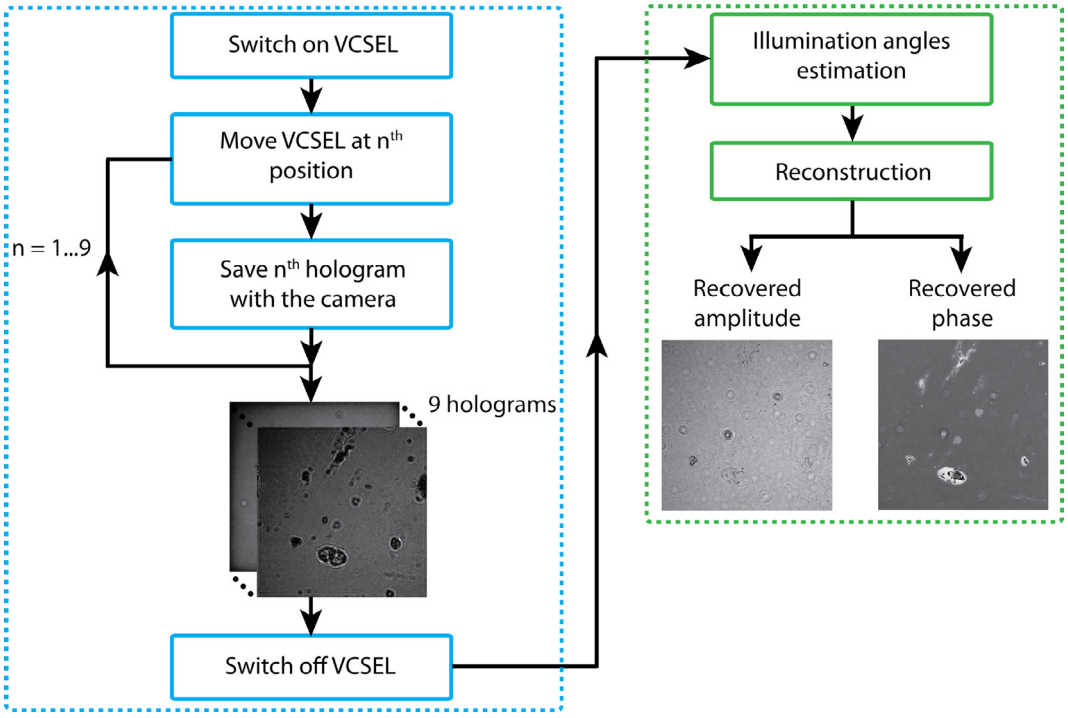


Fig. 4. Acquisition and reconstruction process of the proposed compact in-line lensfree microscope. Acquisition steps are in blue and reconstruction step in green. (For interpretation of the references to colour in this figure legend, the reader is referred to the web version of this article.)

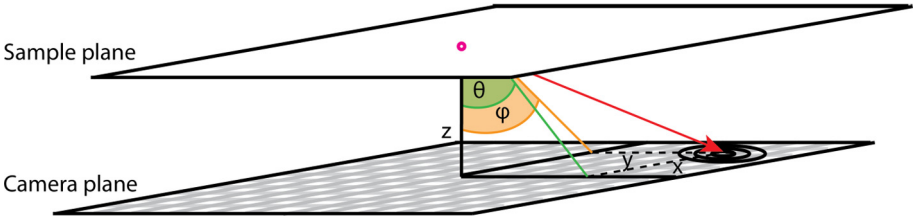


Fig. 5. Illumination angles determination. φ and θ are the angles between the normal to the camera plane and the diffracted beam in x and y directions.

lating a single VCSEL, an array of individually addressable VCSELs would perform the same task but without any moving parts. A user-friendly Labview interface has been implemented to automatize the recording procedure. The program starts by switching on the VCSEL, which is moved to the first position at the entrance surface of the prism. This first position creates a first beam by diffraction off the volume hologram. A first digital hologram is recorded. Then the VCSEL is moved to the second position at the entrance surface of the prism, which creates a second beam by diffraction off the volume hologram. A second digital hologram is recorded. This sequence is repeated for the 9 positions of the VCSEL which corresponds to 9 illumination directions of the sample.

3.2. Image reconstruction

The stack of holograms is then inserted in a registration algorithm [40] in order to extract the 2D shifts of each hologram at the camera plane with respect to the hologram taken with normal incidence. These shifts are then converted in illumination angles using the following equations

$$\varphi = \tan^{-1}\frac{x \times p}{z}; \quad \theta = \tan^{-1}\frac{y \times p}{z}$$

where x (resp.y) is the shift in pixels in one direction (resp. the other one), p is the pixel size and z is the distance between the sample and the camera. Fig. 5 shows the case of one illumination direction.

The algorithm takes the stack of holograms recorded with different illumination directions and iteratively estimates the object phase and amplitude with the help of appropriate proximity operators [41]. The reconstructed object $o^+ \in \mathbb{C}^N$ (where N is the number of pixels) is estimated in a variational framework by minimizing a cost function which is a sum of the likelihood term L and a regularization term R:

$$o^+ = \arg\min_{o \in D^N} L(o) + \mu R(o)$$

where $D = \{x \in \mathbb{C}; |x| = 1\}$ is the subspace of $\mathbb{C}$ of phase only objects. μ is a regularization parameter that tunes the balance between the information given by the measurements and the priors. In this approach known as penalized maximum likelihood, the data term is defined according to the forward model and the statistics of the noise, whereas the regularization function is designed to enforce some prior knowledge about the object (such as support, non-negativity, smoothness,...). In the presented work,

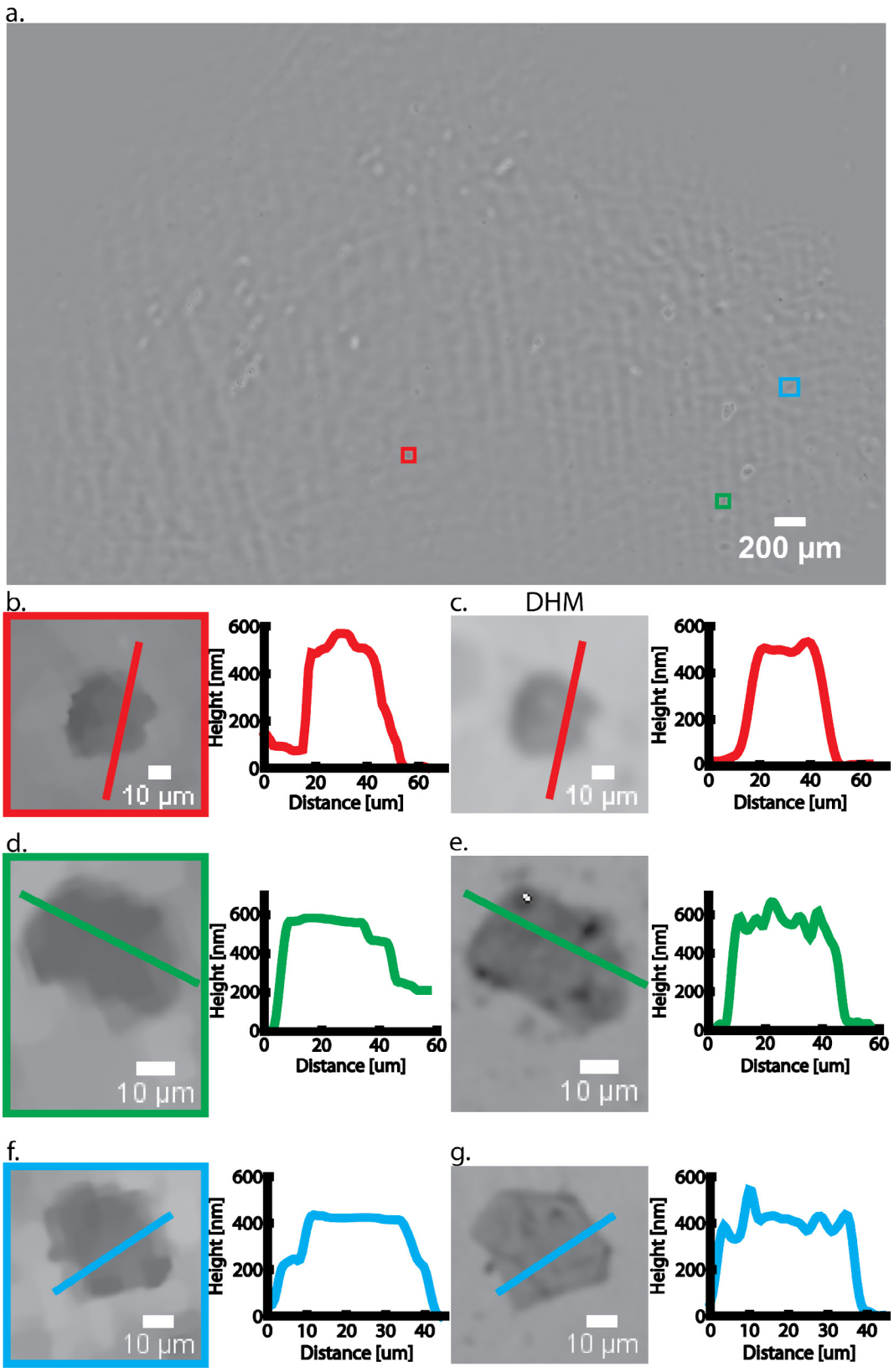


Fig. 6. (a) Reconstructed phase with the proposed device and algorithm full FOV. (b) Reconstructed phase with the proposed device and algorithm (crop from a. of 0.0064 mm^2). (c) Reconstructed phase with a Digital Holographic Microscope (DHM) using a 5× objective (crop 0.0064 mm^2). (d) Reconstructed phase with the proposed device and algorithm (crop from a. of 0.0033 mm^2). (e) Reconstructed phase with a Digital Holographic Microscope (DHM) using a 10× objective (crop 0.0033 mm^2). (f) Reconstructed phase with the proposed device and algorithm (crop from a. of 0.004 mm^2). (g) Reconstructed phase with a Digital Holographic Microscope (DHM) using a 10x objective (crop 0.004 mm^2).

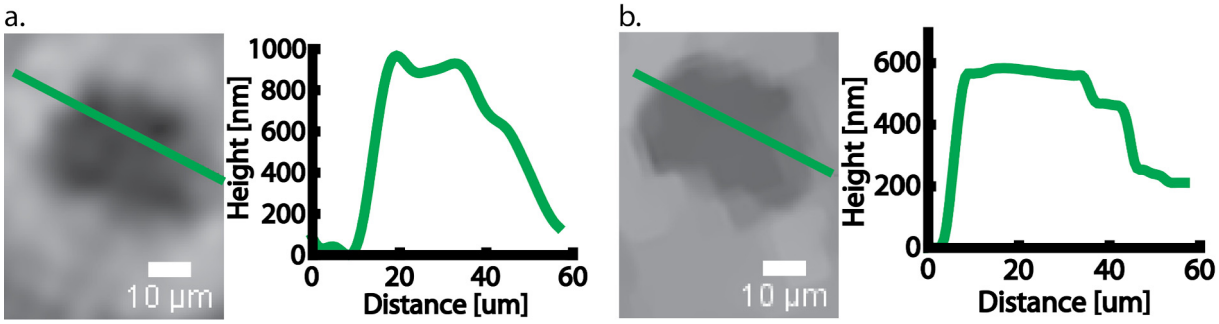


Fig. 7. (a) Reconstructed phase by only backpropagating one hologram recorded with the proposed. (b) Reconstructed phase with the proposed device and algorithm (crop from a. of 0.0033 mm^2).

we use the well-known total variation regularization function [42]. The equation is solved by the mean of the alternating direction method of multipliers (ADMM). It uses a closed form solution for proximity operator of each function [41]. Such an iterative projection method is a Total Variation regularized evolution of the seminal algorithms of Gerschberg Saxon [43] and Fienup [44]. The outputs of the algorithm are the reconstructed amplitude and phase of the sample. In order to obtain quantitative phase results, a calibration of the reconstruction is made using commercial DHM images as references.

All the beams overlap on a ~17 mm^2 FOV, corresponding to ~50% of the camera chip size. This is in the same order of magnitude of FOV demonstrated in [22,23]. However it is larger than classical off-axis scheme since no objective is used.

4. Experimental results

Dried human epithelial cells on a microscope slides were imaged using the presented device with illumination angles ranging between −9° and 9° along both directions. The reconstructed phases from the device using 9 holograms and from a commercial DHM (LynceeTec T1003, 5× and 10× objectives) are shown in Fig. 6. Profile cuts were performed to show the quantitative phase capability of the technique. Using our device, the thickness of the cells can be estimated and is in agreement with the DHM observation. This thickness H is deduced from the phase value using the following equation:

$$H = \frac{\Delta\varphi \times \lambda}{2\pi\Delta n}$$

where, $\Delta\varphi$ is the measured phase in radian, λ is the wavelength in vacuum and Δn is the difference between the refractive index of air and that of the dried cell. The refractive index of the dried cell chosen is 1.3.

However, as the illumination with our device is not as uniform as with a DHM, the reconstructed phase image is noisier and presents some 'pixelation' artifacts and non-uniformity across the full FOV. This last point is not a limitation since a calibration is taking into account this non-uniform illumination. The apparent noisy background of the reconstruction is coming from the illumination beams that suffer from non-uniformities in the photopolymer substrate.

Note that the DHM has a FOV about 4 times smaller with a 5× objective for a similar resolution.

Fig. 7 shows the difference between the reconstructed phase by backpropagating only one hologram (Fig. 7(a)) and by using the proposed algorithm with 9 holograms (Fig. 7(b)). It is clear that the retrieved phase of the first case is not quantitative. The use of the proposed algorithm is relevant.

5. Discussion and conclusions

A compact lensfree in-line digital holographic microscope was presented in this paper. The device is ~10 mm height and easy to use thanks to the user interface. It allows visualizing and measuring the thickness of transparent objects, which can be used to extract different parameters for cells study for example. The device has been tested with a phase only sample and showed good quantitative phase retrieval. We are currently working on the reconstruction algorithm to reduce the artefacts and increase the phase accuracy.

The digital holographic capacity can be combined with another microscopy modality such as fluorescence since the sample is visually accessible from the top of the device. Further work on fabricating a hand-held version of the device is ongoing.

Funding

European Research Council (grant No. 6,92,726 "GlobalBioIm: Global integrative frameworkfor Computational Bio-Imaging").

Acknowledgement

The authors would like to acknowledge Dr. Zahra Monemhaghdoust and Dr. Yves Emery for the images from commercial DHM of LynceeTec.

References

[1] F. Zernike, Phase contrast, a new method for the microscopic observation of transparent objects part II, Physica 9 (1942) 974–986, https://doi.org/10.1016/S0031-8914(42)80079-8.
[2] G. Di Caprio, M.A. Gioffrè, N. Saffioti, S. Grilli, P. Ferraro, R. Puglisi, D. Balduzzi, A. Galli, G. Coppola, Quantitative label-free animal sperm imaging by means of digital holographic microscopy, IEEE J. Sel. Top. Quantum Electron. 16 (2010) 833–840, https://doi.org/10.1109/JSTQE.2009.2036741.
[3] I. Bernhardt, L. Ivanova, P. Langehanenberg, B. Kemper, G. von Bally, Application of digital holographic microscopy to investigate the sedimentation of intact red blood cells and their interaction with artificial surfaces, Bioelectrochemistry 73 (2008) 92–96, https://doi.org/10.1016/j.bioelechem.2007.12.001.
[4] N. Pavillon, A. Benke, D. Boss, C. Moratal, J. Kühn, P. Jourdain, C. Depeursinge, P. J. Magistrettiy, P. Marquety, Cell morphology and intracellular ionic homeostasis explored with a multimodal approach combining epifluorescence and digital holographic microscopy, J. Biophoton. 3 (2010) 432–436, https://doi.org/10.1002/jbio.201000018.
[5] B. Rappaz, A. Barbul, Y. Emery, R. Korenstein, C. Depeursinge, P.J. Magistretti, P. Marquet, Comparative study of human erythrocytes by digital holographic microscopy, confocal microscopy, and impedance volume analyzer, Cytom. Part A 73 (2008) 895–903, https://doi.org/10.1002/cyto.a.20605.
[6] B. Rappaz, P. Marquet, E. Cuche, Y. Emery, C. Depeursinge, P. Magistretti, Measurement of the integral refractive index and dynamic cell morphometry of living cells with digital holographic microscopy, Opt. Express 13 (2005) 9361–9373, https://doi.org/10.1364/OPEX.13.009361.

[7] K.J. Chalut, A.E. Ekpenyong, W.L. Clegg, I.C. Melhuish, J. Guck, Quantifying cellular differentiation by physical phenotype using digital holographic microscopy, Integr. Biol. 4 (2012) 280, https://doi.org/10.1039/c2ib00129b.
[8] J. Kühn, E. Shaffer, J. Mena, B. Breton, J. Parent, B. Rappaz, M. Chambon, Y. Emery, P. Magistretti, C. Depeursinge, P. Marquet, G. Turcatti, Label-free cytotoxicity screening assay by digital holographic microscopy, Assay Drug Dev. Technol. 11 (2013) 101–107, https://doi.org/10.1089/adt.2012.476.
[9] L. Yu, S. Mohanty, J. Zhang, S. Genc, M.K. Kim, M.W. Berns, Z. Chen, Digital holographic microscopy for quantitative cell dynamic evaluation during laser microsurgery, Opt. Express 17 (2009) 12031, https://doi.org/10.1364/OE.17.012031.
[10] B. Kemper, A. Bauwens, A. Vollmer, S. Ketelhut, P. Langehanenberg, J. Müthing, H. Karch, G. von Bally, Label-free quantitative cell division monitoring of endothelial cells by digital holographic microscopy, J. Biomed. Opt. 15 (2010) 36009, https://doi.org/10.1117/1.3431712.
[11] A. Khmaladze, R.L. Matz, T. Epstein, J. Jasensky, M.M. Banaszak Holl, Z. Chen, Cell volume changes during apoptosis monitored in real time using digital holographic microscopy, J. Struct. Biol. 178 (2012) 270–278, https://doi.org/10.1016/j.jsb.2012.03.008.
[12] D. Boss, J. Kühn, P. Jourdain, C. Depeursinge, P.J. Magistretti, P. Marquet, Measurement of absolute cell volume, osmotic membrane water permeability, and refractive index of transmembrane water and solute flux by digital holographic microscopy, J. Biomed. Opt. 18 (2013) 36007, https://doi.org/10.1117/1.JBO.18.3.036007.
[13] B. Rappaz, F. Charrière, C. Depeursinge, P.J. Magistretti, P. Marquet, Simultaneous cell morphometry and refractive index measurement with dual-wavelength digital holographic microscopy and dye-enhanced dispersion of perfusion medium, Opt. Lett. 33 (2008) 744, https://doi.org/10.1364/OL.33.000744.
[14] N. Pavillon, J. Kühn, C. Moratal, P. Jourdain, C. Depeursinge, P.J. Magistretti, P. Marquet, Early cell death detection with digital holographic microscopy, PLoS One 7 (2012) 1–9, https://doi.org/10.1371/journal.pone.0030912.
[15] J. Sheng, E. Malkiel, J. Katz, J. Adolf, R. Belas, A.R. Place, Digital holographic microscopy reveals prey-induced changes in swimming behavior of predatory dinoflagellates, Proc. Natl. Acad. Sci. U.S.A. 104 (2007) 17512–17517, https://doi.org/10.1073/pnas.0704658104.
[16] A. El Mallahi, C. Minetti, F. Dubois, Automated three-dimensional detection and classification of living organisms using digital holographic microscopy with partial spatial coherent source: application to the monitoring of drinking water resources, Appl. Opt. 52 (2013) A68, https://doi.org/10.1364/AO.52.000A68.
[17] S.K. Jericho, P. Klages, J. Nadeau, E.M. Dumas, M.H. Jericho, H.J. Kreuzer, In-line digital holographic microscopy for terrestrial and exobiological research, Planet. Space Sci. 58 (2010) 701–705, https://doi.org/10.1016/j.pss.2009.07.012.
[18] C.J. Mann, L. Yu, M.K. Kim, Movies of cellular and sub-cellular motion by digital holographic microscopy, Biomed. Eng. Online 5 (2006) 21, https://doi.org/10.1186/1475-925X-5-21.
[19] M. Heydt, M.E. Pettitt, X. Cao, M.E. Callow, J.A. Callow, M. Grunze, A. Rosenhahn, Settlement behavior of zoospores of Ulva linza during surface selection studied by digital holographic microscopy, Biointerphases 7 (2012) 1–7, https://doi.org/10.1007/s13758-012-0033-y.
[20] P. Marquet, C. Depeursinge, P.J. Magistretti, Review of quantitative phase-digital holographic microscopy: promising novel imaging technique to resolve neuronal network activity and identify cellular biomarkers of psychiatric disorders, Neurophotonics 1 (2014) 20901, https://doi.org/10.1117/1.NPh.1.2.020901.
[21] R. Barer, Determination of dry mass, thickness, solid and water concentration in living cells, Nature 172 (1953) 1097–1098, https://doi.org/10.1038/1721097a0.
[22] O. Mudanyali, D. Tseng, C. Oh, S.O. Isikman, I. Sencan, W. Bishara, C. Oztoprak, S. Seo, B. Khademhosseini, A. Ozcan, Compact, light-weight and cost-effective microscope based on lensless incoherent holography for telemedicine applications, Lab. Chip 10 (2010) 1417, https://doi.org/10.1039/c000453g.
[23] A. Greenbaum, W. Luo, T.-W. Su, Z. Göröcs, L. Xue, S.O. Isikman, A.F. Coskun, O. Mudanyali, A. Ozcan, Imaging without lenses: achievements and remaining challenges of wide-field on-chip microscopy, Nat. Methods 9 (2012) 889–895, https://doi.org/10.1038/nmeth.2114.
[24] M. Rostykus, F. Soulez, M. Unser, C. Moser, Compact lensless phase imager, Opt. Express 25 (2017) 241–245, https://doi.org/10.1364/OE.25.004438.
[25] U. Schnars, W. Jueptner, in: Digital Holography, Springer-Verlag, Berlin/Heidelberg, 2005, https://doi.org/10.1007/b138284.
[26] U. Schnars, W. Jüptner, Direct recording of holograms by a CCD target and numerical reconstruction, Appl. Opt. 33 (1994) 179–181, https://doi.org/10.1364/AO.33.000179.
[27] N.C. Pégard, M.L. Toth, M. Driscoll, J.W. Fleischer, Flow-scanning optical tomography, Lab. Chip 14 (2014) 4447–4450, https://doi.org/10.1039/C4LC00701H.
[28] M. Rostykus, C. Moser, Compact lensless off-axis transmission digital holographic microscope, Opt. Express 25 (2017) 16652, https://doi.org/10.1364/OE.25.016652.
[29] B. Mandracchia, V. Bianco, Z. Wang, M. Mugnano, A. Bramanti, M. Paturzo, P. Ferraro, Holographic microscope slide in a spatio-temporal imaging modality for reliable 3D cell counting, Lab. Chip 17 (2017) 2831–2838, https://doi.org/10.1039/C7LC00414A.
[30] V. Bianco, B. Mandracchia, V. Marchesano, V. Pagliarulo, F. Olivieri, S. Coppola, M. Paturzo, P. Ferraro, Endowing a plain fluidic chip with micro-optics: a holographic microscope slide, Light Sci. Appl. 6 (2017) e17055, https://doi.org/10.1038/lsa.2017.55.
[31] G. Koren, F. Polack, D. Joyeux, Iterative algorithms for twin-image elimination in in-line holography using finite-support constraints, J. Opt. Soc. Am. A 10 (1993) 423–433, https://doi.org/10.1364/JOSAA.10.000423.
[32] G. Liu, P.D. Scott, Phase retrieval and twin-image elimination for in-line Fresnel holograms, J. Opt. Soc. Am. A 4 (1987) 159, https://doi.org/10.1364/JOSAA.4.000159.
[33] T. Latychevskaia, H.-W. Fink, Solution to the twin image problem in holography, Phys. Rev. Lett. 98 (2007) 233901, https://doi.org/10.1103/PhysRevLett.98.233901.
[34] B.M. Hennelly, D.P. Kelly, N. Pandey, D. Monaghan, Review of twin reduction and twin removal techniques in holography, in: Conf. Proc., 2009, pp. 1–5.
[35] C. Cho, B. Choi, H. Kang, S. Lee, Numerical twin image suppression by nonlinear segmentation mask in digital holography, Opt. Express 20 (2012) 22454–22464, https://doi.org/10.1364/OE.20.022454.
[36] A. Greenbaum, Y. Zhang, A. Feizi, P.-L. Chung, W. Luo, S.R. Kandukuri, A. Ozcan, Wide-field computational imaging of pathology slides using lens-free on-chip microscopy, Sci. Transl. Med. 6 (2014), https://doi.org/10.1126/scitranslmed.3009850. 267ra175-267ra175.
[37] L. Denis, C. Fournier, T. Fournel, C. Ducottet, Twin-image noise reduction by phase retrieval in in-line digital holography, in: M. Papadakis, A.F. Laine, M.A. Unser (Eds.), Wavelets XI, SPIE's Symp. Opt. Sci. Technol., 2005, p. 59140J, https://doi.org/10.1117/12.617405.
[38] C. Zuo, J. Sun, J. Zhang, Y. Hu, Q. Chen, Lensless phase microscopy and diffraction tomography with multi-angle and multi-wavelength illuminations using a LED matrix, Opt. Express 23 (2015) 14314–14328, https://doi.org/10.1364/OE.23.014314.
[39] W. Luo, A. Greenbaum, Y. Zhang, A. Ozcan, Synthetic aperture-based on-chip microscopy, Light Sci. Appl. 4 (2015) e261, https://doi.org/10.1038/lsa.2015.34.
[40] M. Guizar-sicairos, S.T. Thurman, J.R. Fienup, Efficient subpixel image registration algorithms, Opt. Lett. 33 (2008) 156–158.
[41] F. Soulez, É. Thiébaut, A. Schutz, A. Ferrari, F. Courbin, M. Unser, Proximity operators for phase retrieval, Appl. Opt. 55 (2016) 7412–7421.
[42] L.I. Rudin, S. Osher, E. Fatemi, Nonlinear total variation based noise removal algorithms, Phys. D: Nonlin. Phenom. 60 (1992) 259–268, https://doi.org/10.1016/0167-2789(92)90242-F.
[43] R.W. Gerchberg, W.O. Saxton, A practical algorithm for the determination of phase from image and diffraction plane pictures, Optik (Stuttg) 35 (1972) 237–246, https://doi.org/10.1070/QE2009v039n06ABEH013642.
[44] J.R. Fienup, Phase retrieval algorithms: a comparison, Appl. Opt. 21 (1982) 2758–2769, https://doi.org/10.1364/AO.21.002758.